

GRAPE : A STOCHASTIC GEOMETRICAL 3D MODEL FOR AGGREGATES OF PARTICLES WITH TUNABLE 2D MORPHOLOGICAL PROJECTED PROPERTIES

LÉO THÉODON^{✉,1}, CAROLE COUFORT-SAUDEJAUD² AND JOHAN DEBAYLE¹

¹MINES Saint-Etienne, CNRS, UMR 5307 LGF, Centre SPIN, Saint-Etienne, France, ²Laboratoire de Génie Chimique, Université de Toulouse, CNRS, INPT, UPS, Toulouse, France

e-mail: l.theodon@emse.fr, carole.saudejaud@toulouse-inp.fr, debayle@emse.fr

(Received January 18, 2023; revised February 24, 2023; accepted February 24, 2023)

ABSTRACT

The main goal of this paper is to propose a method for the 3D morphological characterization of compact aggregates using 2D image analysis. The problem at hand is, for example, the 3D morphometric characterization of latex nanoparticle aggregates. The only available information is 2D opaque projection images of these aggregates, one projection per aggregate. In this context, a method to estimate the 3D morphological characteristics of an aggregate such as the Volume, Surface Area or Solidity from a single opaque projection is proposed. This method is based on a stochastic geometric model called GRAPE (Geometrical Random Aggregation of Particles Emulation) and requires some strong assumptions, and in particular prior estimation of the volume. The model is based on an iterative packing of spheres of identical radii. For each iteration, a fitting function allows to reach objectives corresponding to the desired 2D properties (Area, Perimeter, Aspect Ratio, ...). In order to implement the method, an optimization process must be performed on two parameters of the model: the radius of the primary particles r and an overlapping distance d_i . As a validation, this process will be applied to synthetic aggregates, themselves generated from the GRAPE model, then to a population of 10^4 synthetic aggregates, and finally to 3D printed aggregates whose 3D morphological properties are known thanks to an STL file, and whose projected images have been produced using a morphogranulometer. The results obtained show an excellent approximation of 2D properties by the GRAPE model, and very good results for 3D properties, with less than 5% error on average and less than 2% error in most cases.

Keywords: 3D stochastic model, agglomerate, aggregate, morphological characterization, stochastic geometry.

INTRODUCTION

The characterization of particle aggregates is a problem being faced in many fields of research. From pharmaceutical industry (Alander *et al.*, 2003; Huo *et al.*, 2016; Mehle *et al.*, 2017) to chemical industry (Wentzel *et al.*, 2003; Maggi *et al.*, 2011; 2015; Lapuerta *et al.*, 2017; Guérin *et al.*, 2019), and from food processing (Faria *et al.*, 2003; Turchiuli and Castillo-Castaneda, 2009; Atalar and Yazici, 2019) to civil engineering (Jin *et al.*, 2019; Wang *et al.*, 2021; Li *et al.*, 2021; Gong *et al.*, 2021), the modeling of aggregation phenomena and the characterization of aggregates requires the ongoing development of new innovative techniques. Depending on the issue and the context, the characterization of aggregates can take different forms. It may involve measuring the geometrical and morphological properties of aggregates, particularly at the millimeter or centimeter scale (Gong *et al.*, 2021), and it may also focus on the size and fractal dimension of aggregates (Guérin *et al.*, 2019). Population balance models (Ramkrishna, 2000; Burd, 2013; Song *et al.*, 2015; Jeldres *et al.*, 2015) are also widely used to

determine mass, shape, or size distributions of a population of aggregates, for example by calculating the Particle Size Distribution (PSD).

Thus, the characterization of aggregates does not correspond to the measurement of a well-defined set of properties, but depends above all on the context in which it is performed. For this reason, it is possible to distinguish two main categories of aggregate characterization techniques: direct methods, where the aim is to directly measure certain characteristics and properties of aggregates using image analysis techniques for instance, and methods based on the modeling of the aggregation phenomenon.

In the case of direct analysis, traditional methods are mainly based on 2D projection image analysis techniques of the aggregates (Ros *et al.*, 1993; Alander *et al.*, 2003; Faria *et al.*, 2003; Pons *et al.*, 2005; Huo *et al.*, 2016; Omar, 2020; Wang *et al.*, 2021) – although techniques based on 3D reconstruction of the aggregates exist at the macroscale (Garboczi, 2002; Turchiuli and Castillo-Castaneda, 2009; Komba *et al.*, 2013) – on which measurements are performed, such as the calculation of the fractal dimension,

Nomenclature			
A_p	Projected area	P	Perimeter
c_k	A given configuration	PAL	Principal axis length
$D_{f,2}$	2D fractal dimension	r	Radius of the primary particles
$D_{f,3}$	3D fractal dimension	r_g	Radius of gyration
d_i	Minimum distance between the centers of two primary particles	S	Surface area
ESD	Equivalent spherical diameter	SLD	Solidity
F	Cost function	v_1, v_2	Random variables
f_{fit}	Fitting function	V	Volume
F_{max}	Maximum Feret diameter	\tilde{V}	Volume estimate
F_{min}	Minimum Feret diameter	V_c	Volume of the convex hull
M_a	Major axis	X, Y	Random variables
m_a	Minor axis	Z	Coordination number
m_i	Center of mass of a particle	ω	Subset of parameters
N_c	Number of configuration	Ψ_{AR}	Aspect ratio
N_p	Number of primary particles	τ	Geometric tortuosity

or the counting of primary particles with circle detection algorithms (Einar Krus *et al.*, 1994) in order to obtain the PSD. More recently, image analysis techniques based on Artificial Neural Networks (ANNs) (Frei and Krus, 2018), Convolution Neural Networks (CNNs) (Mehle *et al.*, 2017; Frei and Krus, 2018; Monchot *et al.*, 2021) and Generative Adversarial Networks (GANs) (Rühle *et al.*, 2021) have been developed, which allows a real-time processing, segmentation, and calculation of the PSD. Nevertheless, these techniques remain limited in terms of number of characteristics that can be measured, in addition to being sometimes computationally expensive, with the exception of neural network-based techniques. Indeed, complex shapes are difficult to process by classical segmentation methods. Moreover, the measured properties are essentially made in 2D.

The modeling of aggregation phenomena provides more complete data regarding the geometrical and morphological characteristics of the aggregates, since the 3D geometry of the latter is known, with the exception of the population balance models, which does not allow for 3D visualization of the aggregates, thus preventing 2D projection images from being generated and measured. Numerous techniques exist outside of population balance models, such as molecular dynamics (Dong *et al.*, 2017; Zheleznyakova, 2021), stochastic processes such as Monte-Carlo (Schmid *et al.*, 2004; Kadota *et al.*, 2011; Hussain *et al.*, 2014; Ono *et al.*, 2015; Morán *et al.*, 2020; Shen *et al.*, 2021), Langevin equations (Henry *et al.*, 2013; Lazzari *et al.*, 2016), and, in a more general way, all techniques based on the framework

of Discrete Elements Methods (DEM) (Shyshko and Mechtcherine, 2013; Spettl *et al.*, 2015; Deng and Davé, 2017; Zhang *et al.*, 2018; Shi *et al.*, 2020). Morán *et al.* (2020) provide in their introduction a fairly complete picture of the models available for simulating nano-particles agglomerates, each of them allowing to model different characteristics of the aggregates, whether it is their shape or size. When it comes to the macroscopic scale, techniques based on parametric shapes are also available (Li *et al.*, 2019).

In this paper, a geometric stochastic model called GRAPE¹ and based on an iterative sphere packing process is proposed for aggregates with a *small* number of particles ($N_p < 1000$). The idea is to be able to control many 2D morphological and geometrical properties of the aggregate, although the model is flexible enough to control virtually any measurable 2D or 3D properties. The model differs from others by its stochastic nature, and the fact that, usually, only the fractal dimension is taken into account when generating an aggregate (Thouy and Jullien, 1994; Morán *et al.*, 2019; Guesnet *et al.*, 2019; Tomchuk *et al.*, 2020; Ferri *et al.*, 2021), in addition to its size.

The proposed model aims at developing a method to approximate the 3D geometrical properties of an aggregate, from a single image of a 2D opaque projection. The problem is part of the broader context of the morphometric characterization of latex nanoparticle aggregates in a Taylor-Couette reactor, which Guérin *et al.* (2017) have shown to take various sizes and shapes, while remaining highly compact and spherical in most cases. Thus, this paper focuses on the particular case of the 3D characterization of compact

¹Geometrical Random Aggregation of Particles Emulation.

aggregates through the calculation of several size and shape metrics (volume, surface area, equivalent diameter, ...) which will be detailed in the following section *Geometrical properties*.

It is important to note that in work, only a single 2D opaque projection is known for each aggregate to be characterized. Indeed, tools of projective stereology and specifically of stereoscopy exist when it comes to characterizing objects (and particularly aggregates) of which several calibrated projections are available (Turchiuli and Castillo-Castaneda, 2009; Liu *et al.*, 2020). Probabilistic tools allowing to characterize a population of objects from a set of projected images also exist, but the characterized objects need to be particularly simple, such as spheroids or ellipsoids (de Langlard *et al.*, 2021), which is not the case for the aggregates of particles considered. For all these reasons, the most relevant approach to characterize the 3D morphology of an aggregate from a single projected image is based on the development of a stochastic geometric model of a 3D aggregate whose 2D morphology can be controlled. Naturally, the fact that the information provided by a single opaque projection is incomplete requires strong assumptions to be made. For this reason, only the case of compact aggregates will be addressed, and a first estimation of the volume will be performed prior to the modeling process, as detailed in the following.

The originality of the paper not only lies in the model itself but also in the method. Indeed, after having performed 2D measurements on the projected image of an aggregate, an optimal set of parameters for the GRAPE model will be obtained using an optimization process. The synthetic aggregates generated by the model will then have 3D properties equivalent to those of the aggregate for which only the 2D geometrical properties are known.

In the following, the usual 2D and 3D geometrical properties that will be used throughout this paper are defined. The GRAPE model is then presented, as well as the main steps of the algorithm for generating a synthetic aggregate. The optimization process is then described in the context of the characterization of compact aggregates. The latter is validated on two synthetic aggregates whose morphology is supervised and then on a population of 10^4 synthetic aggregates generated by the GRAPE model. Finally, the whole method is validated by being applied to the 2D opaque projection image of a 3D-printed aggregate of almost spherical particles whose 3D structure is known and stored in an STL file. The errors between the 3D geometrical properties of the synthetic aggregates and those of the one stored in the STL file are computed and the results are discussed in the last part. Finally,

several perspectives and outlook are proposed in conclusion and the flexibility of the model is illustrated through examples of realizations with different set of parameters.

GEOMETRICAL PROPERTIES

In this section, the 2D and 3D properties that will be measured on the aggregates being studied are defined. When it comes to characterizing a 2D or 3D shape, the context matters significantly. Indeed, in this paper, only compact aggregates will be considered, although the GRAPE model can generate many other types of aggregates, as shown in section *The GRAPE model*. Therefore, some common properties like the convexity, the circularity, or, admittedly less frequent, the porosity, are not mentioned.

2D PROPERTIES

The projection of a 3D aggregate of particles along an arbitrary axis allows to measure 2D properties on the projected shape (Fig. 1a). The definitions of the properties used by the GRAPE model are listed below.

Projected area and perimeter

The projected area A_p and the perimeter P can be measured on the projection of the agglomerate along a certain axis (Fig 1a). Depending on the chosen axis, the measurements can vary significantly, hence a strong need for consistency.

Feret diameters

Ferets diameters are calculated by projecting a 2D shape in all possible directions. The maximum (resp. minimum) Feret diameter F_{\max} (resp. F_{\min}) is given by the maximum (resp. minimum) projected length obtained (Fig. 1b).

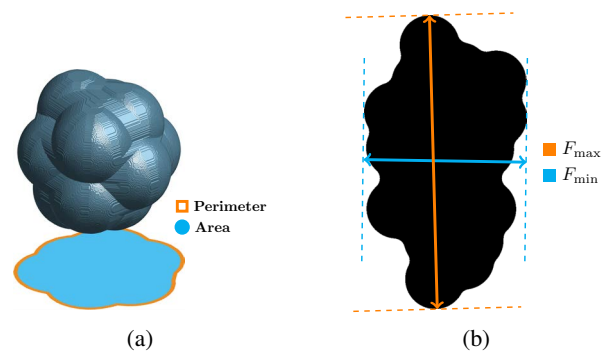


Fig. 1: (a) Illustration of the projected area (blue) and perimeter (red) of a 3D aggregate of spherical particles. (b) Maximum and minimum Feret diameters computed on the 2D projection of the agglomerate.

Aspect ratio

The aspect ratio, usually written Ψ_{AR} , is derived from the Feret diameters as follow.

$$\Psi_{AR} = F_{\min}/F_{\max} \quad (1)$$

which means that $\Psi_{AR} \in [0; 1]$.

Fractal dimension

There are many different definitions of the fractal dimension $D_{f,2}$ (or $D_{f,3}$) of a 2D (or 3D) shape (Samson *et al.*, 1987; Suzuki *et al.*, 1990; Kaye, 1994; Kindratenko *et al.*, 1996; Gmachowski, 2002; Bushell *et al.*, 2002; Berg and Sorensen, 2013; Florio *et al.*, 2019). The Minkowski-Bouligand dimension (Falconer, 1990), also called Kolmogorov capacity (Tikhomirov, 1993), will be computed with the box-counting method described by Li *et al.* (2009).

3D PROPERTIES**Volume**

The volume V of an aggregate is usually computed by summing a number of voxels in a discrete space.

Convex volume

The convex volume V_c is defined as the volume of the convex hull of an object.

Solidity

The solidity $SLD \in [0; 1]$ is defined as the ratio of the volume V over the convex volume V_c , ie

$$SLD = \frac{V}{V_c}. \quad (2)$$

A low solidity might indicated a highly porous, crumbly or brittle material.

Surface area

The surface area S is defined as the area covering the outside of the 3D shape.

Equivalent diameter

The equivalent diameter or equivalent spherical diameter (ESD) is defined as the diameter of a spherical particle of same volume and is computed as follow.

$$ESD = \sqrt[3]{\frac{6 \times V}{\pi}} \quad (3)$$

Principal axis length

The principal axis length (PAL) corresponds to the length of the major axis of an ellipsoid that would have the same co-variant matrix (or normalized second central moment) as the 3D shape.

THE GRAPE MODEL**MODEL'S DESCRIPTION**

The Geometrical Random Aggregation of Particles Emulation (GRAPE) model is designed to generate aggregates of spherical particles whose number varies from a few dozens to a few hundreds, in order to keep good performances. The model is based on an iterative process. At each step, a particle is added to the aggregate, while aiming to minimize a fitting function (see equation (4)). As the real aggregates to be simulated in the scope of this study are only known through 2D opaque projections, the fitting function features properties that can be computed on these projections, such as the projected area A_p , the perimeter P and the aspect ratio Ψ_{AR} . Nevertheless, in a broader framework, any measurable property can be added to the fitting function as discussed in the conclusion of this paper.

Table 1 lists the input parameters of the GRAPE model. It includes the radius r of the primary particles, as well as the minimum distance d_i separating the centers of these particles. The projected area A_p , perimeter P and aspect ratio Ψ_{AR} targets are also listed, as well as the volume V . As a matter of fact, in this work, the stopping criterion used to end the iterative process will be based on an estimate of the volume of the aggregate, rather than by a fixed number of particles to reach.

Table 1: *Listing of the GRAPE model parameters.*

Parameters	Definition
r	Radius of the particles
d_i	Minimum distance between the centers of two particles
A_p	Projected area
P	Perimeter
Ψ_{AR}	Aspect ratio
V	Volume

DESCRIPTION OF THE ALGORITHM

The main steps of the algorithm are described below and illustrated by a flow diagram in Fig. 2.

1. Initialize the model parameters r and d_i and define a set of goals to be reached (a projected area A_p , a perimeter P and an aspect ratio Ψ_{AR}) as well as a volume V . A number of configuration N_c to be tested for each iteration is also defined.
2. The fitting function is then defined as

$$f_{\text{fit}}(c_k) = \Delta(A_p) + \Delta(P) + \Delta(\Psi_{AR}) \quad (4)$$

where Δ represents the relative error between the measured property for the configuration c_k and the corresponding goal set beforehand. The properties of each configuration are 2D morphological properties and are thus computed on 2D projection images, always made in the same direction.

3. Set a first particle and then, for each iteration j , a number N_c of random configurations c_k are tested for the placement of a new particle. Each new particle must be adjacent to an existing particle, and must be at a distance greater than d_i from any other particle. A candidate position for a new particle is chosen randomly and uniformly around the particle to which it is attached.
4. The score $f_{fit}(c_k)$ of each eligible configuration c_k , with $k \in \{1; N_c\}$, is computed and the configuration of minimum score is chosen.
5. The algorithm stops when the stopping criterion is reached, which is a maximum volume V .

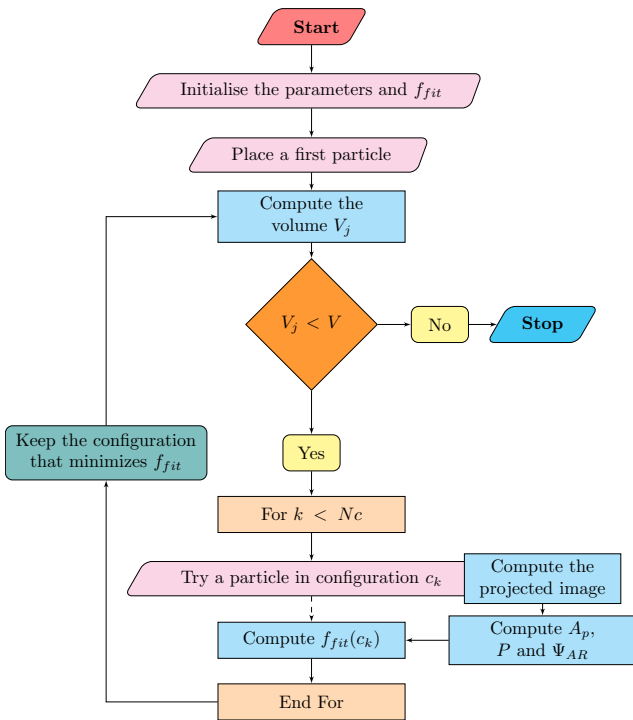


Fig. 2: Flow diagram of the algorithm used by the GRAPE model.

Two observations should be made regarding the proposed algorithm. First, a limited number N_c of configurations are tested for each iteration. While it seems obvious that testing too few configurations can be problematic, the total number of particles constituting the aggregates generated in this work being of the order of a few hundred, it appeared that a number of configurations to be tested of the order of a

few hundred was sufficient, in the sense that increasing N_c beyond a certain threshold did not change the results obtained but only slowed down the process of generating an aggregate. Also, in practice, the number of configurations is set at $N_c = 10^3$. This choice is being discussed in the last section of this paper.

Second, although no 3D information is known about the aggregate we seek to characterize, an assumption must be made about its volume V so as not to generate aggregates like those shown in Fig. 3. Indeed, the reason why the volume is taken into account is to avoid generating flat (Fig. 3a) or highly elongated (Fig. 3b) degenerate aggregates. Nevertheless, as it is impossible to know the real volume V of the aggregate of which only a single 2D opaque projection is available, an estimator \tilde{V} is defined as the volume of an ellipsoid with a major axis equal to M_a and the other two axis equal to m_a , where M_a and m_a are respectively the major and minor axis of the equivalent ellipse, which is an ellipse that has the same area and perimeter as the ones measured on the opaque projection image.

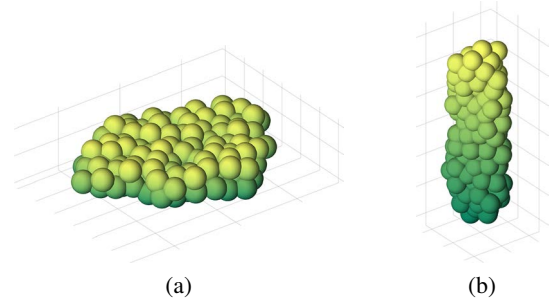


Fig. 3: Examples of degenerate cases of aggregates generated by the GRAPE model with the same goals of projected areas, perimeters and aspect ratio measured along a given direction. Only the particle radius r and the stopping criterion (volume V) differ.

OPTIMIZATION & VALIDATION

The reason why the GRAPE model was developed is to be able to retrieve the 3D properties of an aggregate from a 2D opaque projection image. Thus, the idea is to apply an optimization process to ensure that the characteristics of the 2D projections of the synthetic aggregates generated by the model match those of the observed aggregate. Once an optimal model parameterization has been determined, it can be assumed that the synthetic aggregates have the same 3D characteristics as the desired aggregate. Although matching the projected 2D characteristics of the aggregates does not necessarily lead to matching the

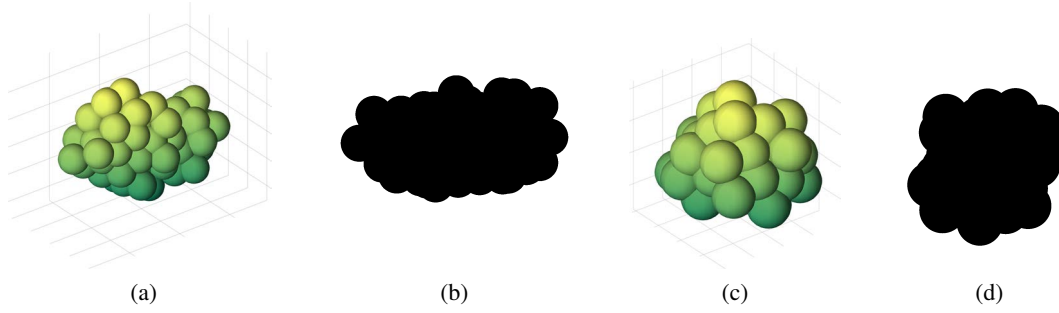


Fig. 4: (a) and (c): Synthetic 3D aggregates generated by the GRAPE model with the sets of parameters ω_0 and ω_1 respectively, and their respective 2D projections (b) and (d) as binary images. (Pictures are not to scale.)

3D characteristics, since a single opaque projection is considered during the process, the strong assumptions that are made, in particular the volume estimation and the compactness of the modeled aggregates, will allow the validation of the proposed method. First, a framework for the optimization process must be established and, more specifically, a cost function to be minimized must be defined.

DEFINITION OF THE COST FUNCTION

Given a subset of parameters $\omega = \{r, d_i\}$ for the GRAPE model, the cost function is defined as followed

$$F(\omega) = \Delta(V) + 8 \times \Delta(A_p) + 8 \times \Delta(P) + 3 \times \Delta(\Psi_{AR}) \quad (5)$$

with V an estimate the 3D volume of the aggregate, A_p the projected area, P the perimeter, and Ψ_{AR} the aspect ratio. The weights assigned to the respective costs were determined empirically.

Note that the cost function is not only based on 2D properties, but also takes into account the 3D volume of the synthetic aggregate generated with the subset of parameters ω .

VALIDATION PROCESS

Validation on a single aggregate

In this section, the method will be applied to two synthetic aggregates generated by the GRAPE model from two distinct sets of parameters (Fig. 4). The idea is to retrieve these two sets of parameters from a single opaque projection for each of these aggregates by applying the method and the optimization process described above. The method applied can be described as follows for each of the two synthetic aggregates.

1. A set of parameters $p = \{r, d_i, A_p, P, \Psi_{AR}, V\}$ is used to generate a synthetic aggregate with the GRAPE model.

2. A projected image of the aggregate is produced. The projection direction is the same as the one used by the GRAPE model.
3. Area, perimeter and aspect ratio measurements are made from the projected image and an estimation of the volume V is also made from the principal axis lengths. This constitutes a first set of estimated parameters $\{\hat{A}_p, \hat{P}, \hat{\Psi}_{AR}, \hat{V}\}$.
4. The GRAPE model being able to generate an aggregate from a set of parameters $p = \{r, d_i, \hat{A}_p, \hat{P}, \hat{\Psi}_{AR}, \hat{V}\}$, an optimization process is then applied to the subset of parameters $\omega = \{r, d_i\}$ using the cost function F defined previously.

In practice, the cost function F is minimized using a simulated annealing algorithm. For each set of parameters ω , a total of 96 realizations are generated using the GRAPE model and the cost function compares the averages of the characteristics of the 96 aggregates to the expected characteristics.

Table 2: Comparison of the sets of parameters used to generate the synthetic 3D aggregates of Fig.4 with the estimators returned by the optimization process.

Parameters	r	d_i
Original values (ω_0)	6	10.2
Fitted values ($\hat{\omega}_0$)	6.01	9.7
Error	0.3%	5%

(a) Fitting of Fig. 4a

Parameters	r	d_i
Original values (ω_1)	8	12
Fitted values ($\hat{\omega}_1$)	8.04	11.3
Error	0.5%	6%

(b) Fitting of Fig. 4c

Table 2 shows the results obtained by the optimization process. The fact that the relative errors

are extremely close is a first validation of the optimization process. In the following section, the method is generalized to a population of aggregates rather than a single aggregate. Joint distributions of 2D morphological characteristics are also used instead of fixed values.

Validation on a population of aggregates

In this section, we repeat the optimization process but this time using a population of aggregates instead of a single aggregate. The population of aggregates counts 10^4 synthetic aggregates and is generated as follows.

Consider two random variables v_1 and v_2 such as

$$v_1 \sim \text{Beta}(2,5) \quad \text{and} \quad v_2 \sim \text{Beta}(5,5) \quad (6)$$

where Beta is the beta distribution of the first kind.

Two other random variables X and Y are then defined by

$$X = 40 + 20v_1 \quad \text{and} \quad Y = 20 + 10v_2 + 30\sqrt{v_1}. \quad (7)$$

Four random variables corresponding to the aspect ratio, the area, the perimeter and an estimate of the volume are then defined as follows

$$A_p = \frac{\pi}{4} \times X \times Y$$

$$P = 2\pi \sqrt{\frac{X^2 + Y^2}{8}}$$

$$\Psi_{AR} = \frac{\min(X,Y)}{\max(X,Y)}$$

$$V = \frac{4}{3}\pi \frac{X^2 \times Y}{8}$$

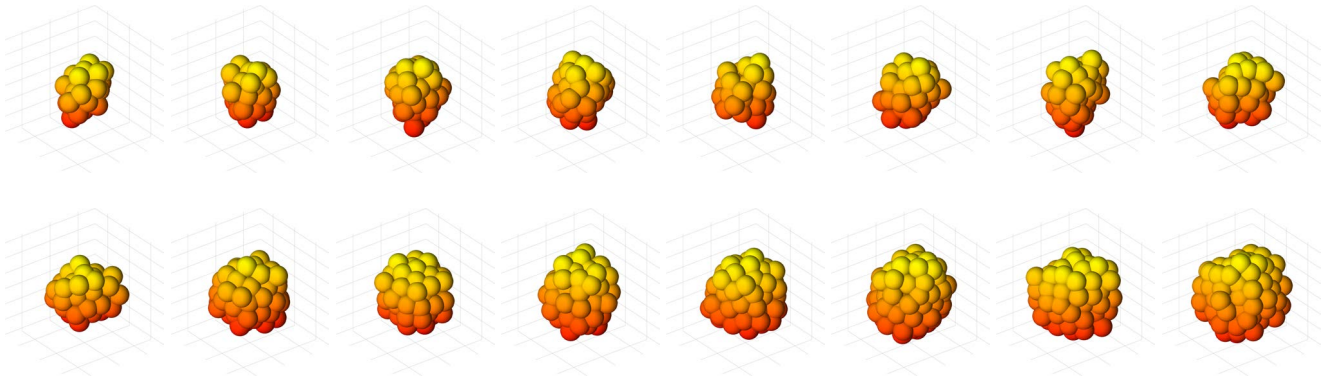


Fig. 6: Examples of aggregates generated by the GRAPE model to create a representative population of size 10^4 . According to the joint probability densities used, the larger the aggregates, the more spherical they are.

Thus, these four characteristics depend on joint probability densities. For example, Fig. 5 shows the joint distribution of aspect ratio and area, which tends to give some physical meaning to the population of aggregates. Indeed, the smaller the projected area, the more elongated the particle.

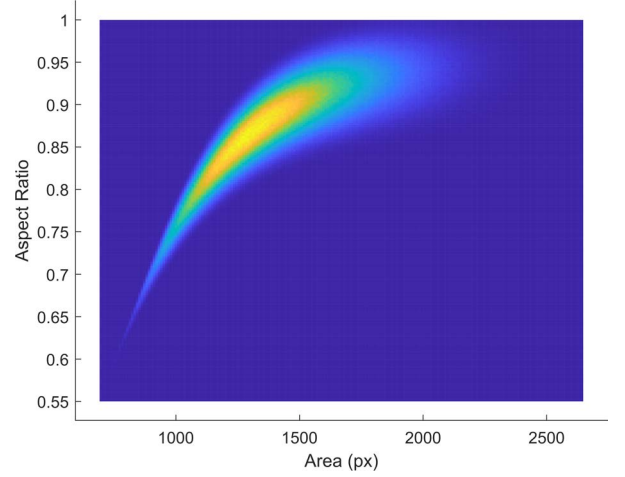


Fig. 5: Joint distribution of area and aspect ratio.

Therefore, when generating the population of 10^4 synthetic aggregates, the joint distributions are used. The result is shown in Fig. 6. The optimization process is then carried out as follows.

1. A set of 10^4 projected images is created from the population of aggregates.
2. On each of the images, measurements of area, perimeter and aspect ratio are performed. A volume estimation is also computed, as described above.
3. The measurements performed on the set of projected images allow to approximate the

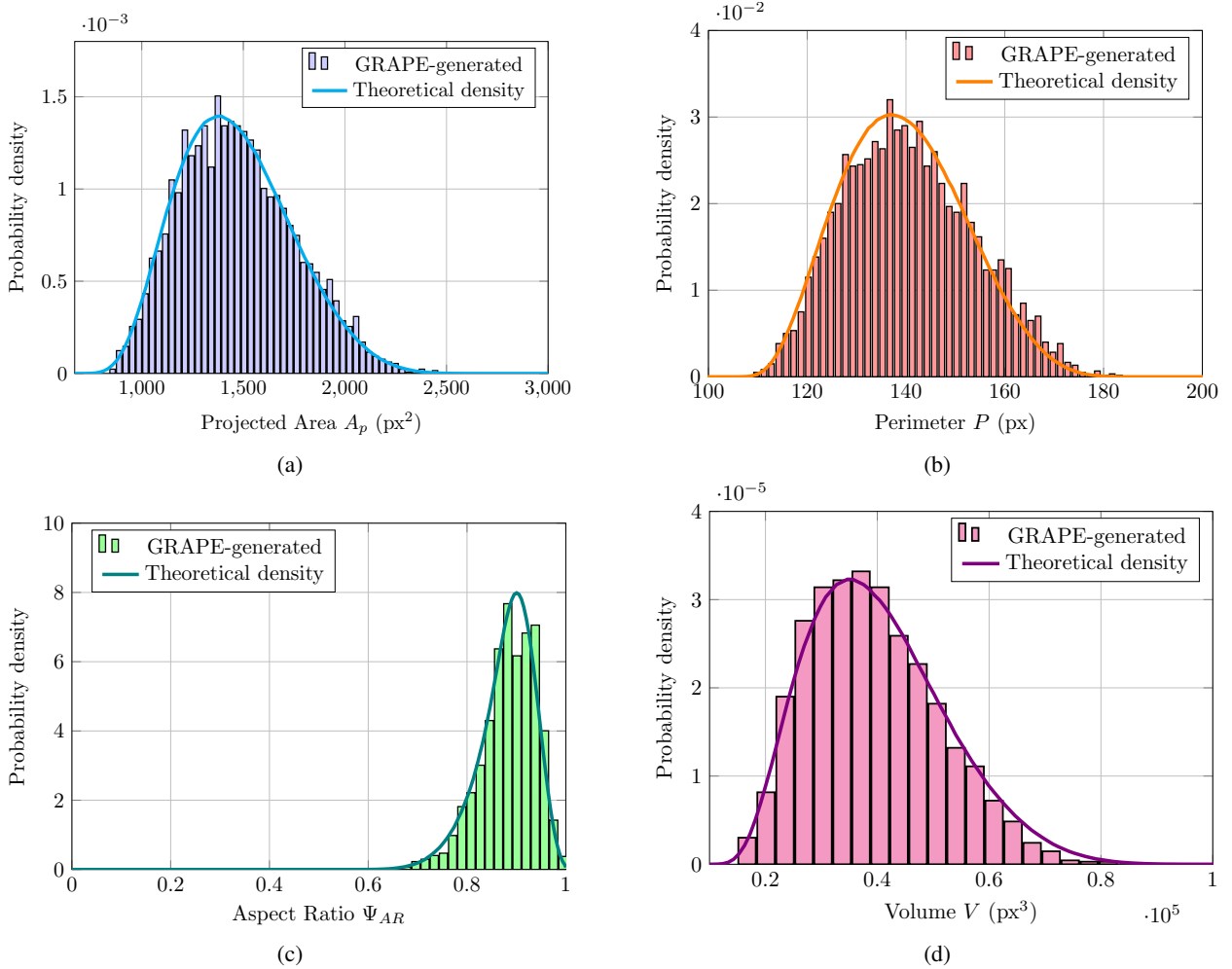


Fig. 7: Theoretical marginal laws of the joint probability densities used to generate a population of 10^4 synthetic aggregates with the set of parameters ω_i versus histograms of measurements performed on the synthetic aggregates proposed by the GRAPE model at the end of the optimization process, with the set of parameters $\hat{\omega}_i$.

corresponding joint probability densities. These approximations of the probability densities compose four of the input parameters of the GRAPE model.

4. The optimization process described in the previous section is once again applied to the remaining parameters to be determined: r and d_i .
5. For each pair of parameters $\omega = \{r, d_i\}$ tested by the optimization process, 1000 realizations of the GRAPE model are performed. The average properties are computed and compared to the averages of the area, perimeter, aspect ratio and estimated volume distributions.

As it can be seen in Table 3, the relative errors between the initial set of parameters $\omega_i = \{r, d_i\}$ and its estimator $\hat{\omega}_i$ resulting from the optimization process are rather small, which implies that the later is indeed

robust and efficient.

Table 3: Comparison of the sets of parameters ω_i used to generate the population of 10^4 synthetic 3D aggregates with the estimator $\hat{\omega}_i$ returned by the optimization process.

Parameters	r	d_i
Original values (ω_i)	6	9
Fitted values ($\hat{\omega}_i$)	6.1	8.9
Relative Error	1.6%	1.1%

Moreover, because the relative errors are so small, the aggregates generated by the GRAPE model from the estimator $\hat{\omega}_i$ have 3D geometrical properties that are necessarily very close to those of the population of 10^4 aggregates, as can be seen for the volume on Fig. 7d. It is also possible to observe (Fig. 7) that

the marginal laws of the theoretical joint probability densities are very well approximated by the histograms produced by the GRAPE model after the optimization process.

After demonstrating that the GRAPE model is efficient when it comes to retrieving the 3D geometrical properties of synthetic aggregates that it has itself generated, the next step is to use aggregates whose 3D geometrical properties are known, but which have not been generated by the GRAPE model. It is the validation step.

RESULTS

In this section, an STL file that contains data for a 3D printer is used. This data contains the structure of a compact aggregate of nearly spherical particles. The idea is to work on a set of 2D opaque projection images of the particle aggregate, and then to use the GRAPE model in order to try to retrieve the 3D data contained in the STL file (Fig. 8).

In practice, a dozen aggregates were 3D printed from the reference STL file. A little more than a thousand images of 2D opaque projections of these aggregates were produced using a morphogranulometer (Morphologi G3 – Malvern

Panalytical). The optimization process described earlier will be applied to this set of images, in order to try to retrieve 3D characteristics of the aggregates, such as the volume or the surface area, which are known thanks to the information contained in the STL file.

The average values of projected area, perimeter and aspect ratio are computed on the images from the morphogranulometer (Fig. 8b). The axes of the equivalent ellipse are also computed in order to propose an estimate of the volume \hat{V} as described previously and used in equation (5). These average values and the volume estimate are used to compute the relative errors in the cost function. To define the goals for the GRAPE model, the whole data set is used, by considering the histograms as probability densities functions.

The cost function is then minimized and the results obtained for the optimal set of parameters $\hat{\omega}$ is presented in Table 4. Since the reference STL file is known, it was possible to make an estimate of the average particle size used during the 3D printing process of the aggregates. It is then possible to compare this estimate to the one proposed by the GRAPE model at the end of the optimization process,

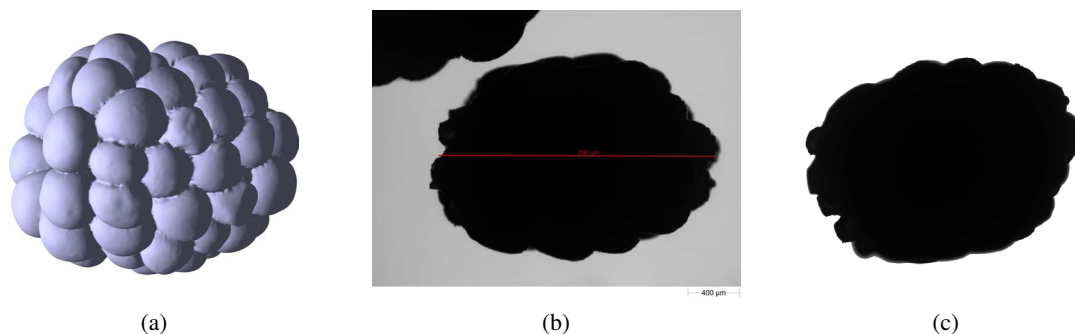


Fig. 8: 3D visualization of the reference STL file (a). Image of a 2D opaque projection from a morphogranulometer of a 3D printed aggregate based on the STL file (b). The aggregates are isolated and the images cleaned before segmentation (c). It is then possible to perform 2D characteristics measurements.

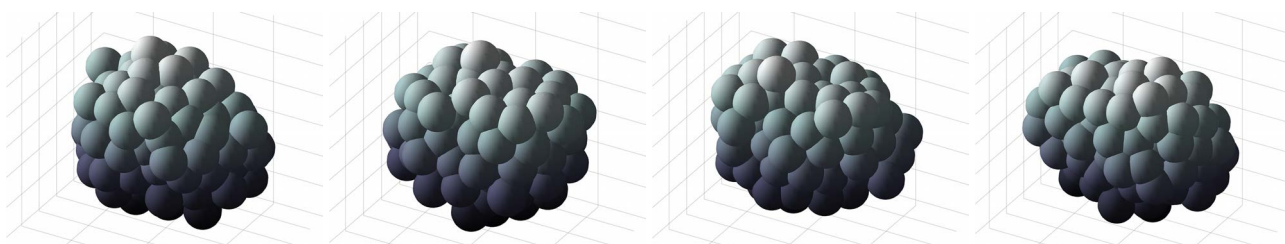


Fig. 9: Examples of realizations from the GRAPE model, with the parameters of Table 4 resulting from the optimization process: $\hat{\omega} = \{191, 309.5\}$.

the relative error being about 0.2%. This result tends to confirm the validity and robustness of the method.

Table 4: *Set of optimal parameters $\hat{\omega}$ for the GRAPE model resulting from the optimization process for the fitting of the 2D projections. Comparison with an estimation of the radius of the particles performed by image analysis.*

Parameters	r (μm)	d_i (μm)
Fitted values ($\hat{\omega}$)	191	309.5
Estimated values	191.3	-

Examples of realizations generated by the GRAPE model from the optimal set of parameters $\hat{\omega}$ are shown in Fig. 9. Table 5 shows the discrepancies between the 2D and 3D measurements made from the 3D aggregate model from the STL file. The properties of the 2D opaque projections are very close, with less than 2% error in each case. The 3D properties are also quite similar, with the exception of the convex volume V_c and, therefore, the solidity SLD. The fact that the volume V is underestimated is partly due to the fact that the 3D volume generated by the GRAPE model may contain holes, which is not the case for the STL file. This hypothesis is all the more plausible as the surface area S is overestimated. As for the equivalent diameter and fractal dimension, they are very well approximated, with also a discrepancy of less than 2%. Regarding the principal axis length measurements, the errors remain relatively small, especially for the main axis. The higher errors for the other two axes is certainly mainly due to the fact that the method of generating the aggregate assumes a certain symmetry in their directions, whereas a more detailed analysis of the data shows that a certain asymmetry exists. Nevertheless, in order to obtain better results, especially in terms of volume and surface area, a post-processing step can be performed.

Table 5: *Comparison of the average 2D (projected) and 3D geometrical properties of the reference aggregate and the aggregates generated by the GRAPE model at the end of the optimization process, with the optimal set of parameters $\hat{\omega} = \{191, 309.5\}$. The values given for the synthetic aggregates generated by the GRAPE model correspond to averages over a set of 4000 realizations.*

Properties	2D				3D				(mm)				
	A_p (mm^2)	P (mm)	Ψ_{AR}	$D_{f,2}$	V (mm^3)	V_c (mm^3)	S (mm^2)	SLD	ESD	PAL ₁	PAL ₂	PAL ₃	$D_{f,3}$
Ground truth	2.73	6.75	0.71	1.53	2.34	2.76	11.25	0.84	1.65	1.98	1.54	1.52	2.1
GRAPE model	2.79	6.78	0.72	1.52	2.24	2.85	11.57	0.78	1.62	1.95	1.65	1.43	2.0
Error (%)	1.7%	0.5%	1.2%	0.3%	4.3%	4.9%	2.9%	7.1%	1.4%	1.4%	7.1%	6.1%	1.5%
	GRAPE + Post-processing				2.307	2.85	11.05	0.81	1.65	1.98	1.66	1.45	2.2
	Error (%)				1.3%	4.9%	1.7%	3.5%	0.4%	0.1%	7.7%	4.8%	1.4%

Post-processing

In order to take into account the fact that the aggregates generated by the GRAPE model contain holes, contrary to the one stored in the STL file, a morphological operation of *hole filling* is performed on the synthetic aggregates (see Soille (2003)). The 3D geometrical properties of the aggregates after this post-processing are also shown in Table 5. The properties are almost identical, with the noticeable exception of the volume which is now much closer to the correct value as well as the surface area which has slightly decreased, as expected, with an error of less than 2% in both cases.

DISCUSSION

The results presented in section *Optimization & Validation* show that it is indeed possible, to a certain extent, and in the case of a compact aggregate of spherical particles, to obtain good approximations of the 3D geometrical properties of the aggregate from measurements performed on a 2D opaque projection, with the help of the GRAPE model. The case studied is somewhat limited, since assumptions are made about the structure of the aggregate, its volume, its compactness in the broad sense, and more generally, its shape: the aggregate is assumed to be compact, and an estimation of its volume is needed as a stopping criterion.

Furthermore, the fact that the convex volume and principal axis lengths cannot be perfectly approximated also illustrates a limitation of the model. Regarding the convex volume, two main assumptions can be made. First, it seems clear that the particles used in the 3D printing of the calibrated aggregates are neither perfectly spherical nor all the same size. This can lead to variations on the surface of the aggregates which will, in fact, alter their structure and convexity. Secondly, it is possible that at the end of the process

of generating a synthetic aggregate using the GRAPE model, one or more spheres are placed at locations that will significantly alter the convex envelope of the aggregate, without having any significant influence on the other characteristics. One way to deal with this issue is to ignore the extreme values when computing the average convex volume. However, although this method gives better results, the threshold at which a value becomes an outlier is not obvious.

That being said, the GRAPE model offers very satisfactory performances, both on the self simulated data and on the data from the STL file recovered from the morphogranulometer images. In each of those cases, the 3D properties of the aggregates were known, and could be compared to the simulated data. Bearing this in mind, it is also important to emphasize the fact that the 3D printed aggregates all present slight variations, and therefore their 2D and 3D characteristics differ slightly from the ground truth provided by the reference STL file. This last point may also explain some of the discrepancies between the synthetic aggregates and the theoretical values.

In the future, it will be important to apply this method to 2D opaque projections of real aggregates, whose 3D geometric properties are unknown. It will also be possible to extend the model to aggregates of spherical particles of variable radius as well as to non-compact aggregates. Following this last point, the flexibility of the GRAPE model is illustrated in the next section.

ON THE GRAPE MODEL

The versatility of the GRAPE model allows it to generate many different configurations of aggregates. Indeed, in this paper, the fitting function f_{fit} only took into account the relative errors of morphological

characteristics computed on a 2D opaque projection. The stopping criterion could also be defined according to a maximum number of particles N_p and no longer be based on a volume V .

Nevertheless, it is possible to build very different aggregates by modifying the fitting function and by taking into account other properties. It is for example possible to consider the coordination number Z which is the average number of contacts per particle, or the radius of gyration r_g which is the square root of the average of the square distance r_i^2 of every mass m_i to the center of mass, weighted by their respective mass m_i , ie

$$r_g = \sqrt{\frac{\sum_i m_i r_i^2}{\sum_i m_i}} \quad (8)$$

according to the IUPAP² definition (McNaught and Wilkinson, 1997).

Finally, if fiber-like aggregates can be generated by choosing a rather small coordination number ($Z \in \{2;3\}$), it is possible to indirectly act on their tortuosity τ^3 by taking the angle α_e between the ends of the fiber and its center of mass into account in the fitting function.

Fig. 10 illustrates some of these possibilities, by adjusting the number of coordination Z or the radius of gyration r_g . As expected, the aggregate is more and more compact as Z increases. The model parameters have a highly noticeable impact on the structure of the aggregates as well as a direct influence on their geometrical properties.

Regarding the performances of the algorithm, it is worth mentioning that the choice of the goals to be reached are decisive in terms of computing time. Indeed, the computation of characteristics performed on 2D opaque projections, such as the projected

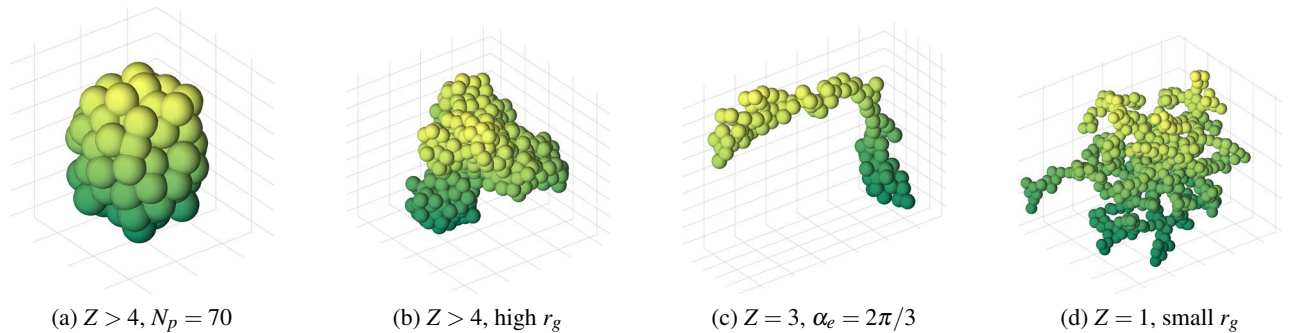


Fig. 10: Example of aggregates generated by the GRAPE model, with various sets of parameters.

²The International Union of Pure and Applied Physics.

³The geometric tortuosity of a fiber-like aggregate is the ratio between its full length and the length of shortest path between its two ends.

area, perimeter, or tortuosity, is much more time consuming and costly than the computation of the coordination number or the radius of gyration. Thus, for an aggregate of a hundred particles, the generation time is on the order of a millisecond when the goals set are *easy* to compute, and on the order of a second when they involve lots of characteristics measured on 2D projections.

In practical terms, the GRAPE model being coded with MATLAB® the generation of 4000 aggregates to produce the data in Table 5 took slightly less than an hour on a machine equipped with an Intel(R) Core(TM) i9-12900KF processor at 3.19Ghz and 64GB of RAM.

ON THE NUMBER OF CONFIGURATIONS

When defining the GRAPE model, it is mentioned that the number of configurations N_c tested at each iteration is set at $N_c = 10^3$. This number of configurations has indeed an influence on the accuracy of the results with respect to the number of particles N_p forming the final aggregate.

Fig. 11 shows the evolution of the relative errors on projected area A_p , perimeter P and aspect ratio Ψ_{AR} as a function of the number of configurations tested for aggregates of different sizes. The curves are displayed as $-\log_{10}[\Delta(C)]$ where $\Delta(C)$ is the relative error on the morphological characteristic $C \in \{A_p; P; \Psi_{AR}\}$ with respect to the goals set prior to the aggregate generation. Thus, a value greater than 1.7 ensures a relative error of less than 2%⁴ when a value greater than 2 gives a relative error smaller than 1%.

As the aggregates studied in this article count less than 150 primary particles and in order to reach a good

⁴ $-\log_{10}(0.02) \approx 1.7$.

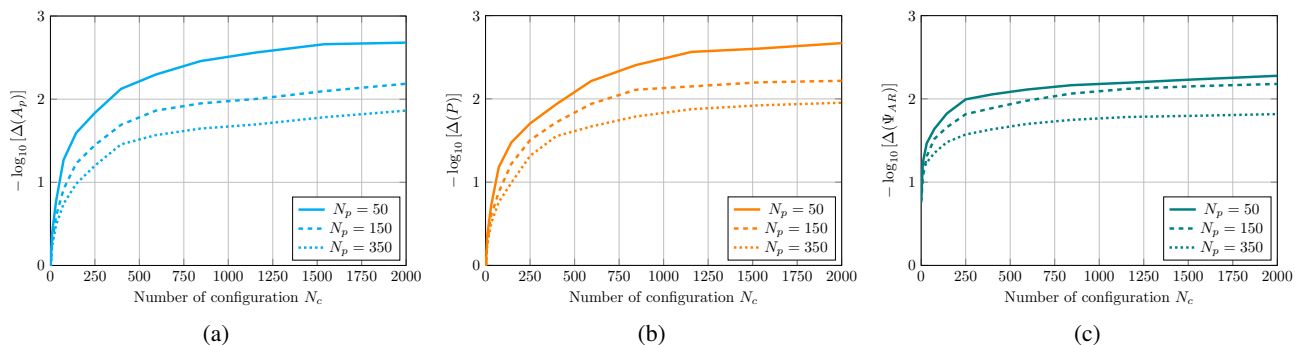


Fig. 11: Evolution of relative errors as a function of the number of configurations tested N_c for aggregates with various numbers of particles N_p . Relative errors are calculated from average values obtained on sets of 200 synthetic aggregates.

compromise between performance and accuracy, the choice was made to set the number of configurations tested per iteration N_c to 10^3 .

ON THE VOLUME ESTIMATE

The estimate \tilde{V} of the volume V of the real aggregate given by the equivalent ellipse of the shape obtained by its 2D opaque projection image allows to define a stopping criterion of the generation process of a synthetic aggregate and is also used in the cost function F of Equation (5). Some ideas have been explored to get around this volume estimate.

First, the stopping criterion can be defined as the number of primary particles N_p . The latter becomes a parameter of the model to be optimized by the cost function F . In this case, in order to maintain a certain cylindrical symmetry of the aggregate, the projections done at each iteration are performed in random directions uniformly over the unit circle. Since the volume estimate cannot be used to define the cost function F , only the 2D morphological characteristics are taken into account. Unfortunately, this method does not allow to correctly approximate either the 2D (Fig. 12) or 3D morphological characteristics of the aggregate. Fig. 12 clearly illustrates the fact that regardless of the number of primary particles N_p , for a fixed set of 2D morphological characteristics, the relative errors are nearly 10 times larger than with the volume estimation method.

Another idea is the multiplication of the number of projections performed at each iteration. Increasing the number of projections in random directions provides better results compared to using a single random projection. However, several dozens of projections per iteration are required before obtaining results

roughly comparable to the volume estimation method. This means a significant loss of performance as the generation of a projected image and the calculation of morphological characteristics is very time consuming. Therefore, for accuracy, efficiency and performance reasons, the method based on the volume estimate was favored.

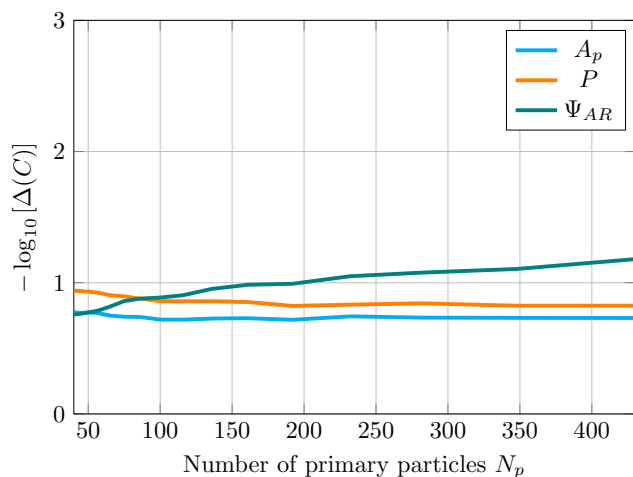


Fig. 12: Relative errors as a function of the number of primary particles N_p made on a fixed set of 2D morphological characteristics $C \in \{A_p; P; \Psi_{AR}\}$ with the first method described to avoid the volume estimation. Number of configurations $N_c = 10^3$ and average over a set of 200 realizations.

EXTENSION

Finally, the GRAPE model can also be extended to the case of spherical particles of variable radius. Although this case is beyond the scope of this paper, it is possible to generate aggregates of particles whose size follows a predefined probability law, as can be seen in Fig. 13 where aggregates are generated from particles whose radii follow a log-normal law.

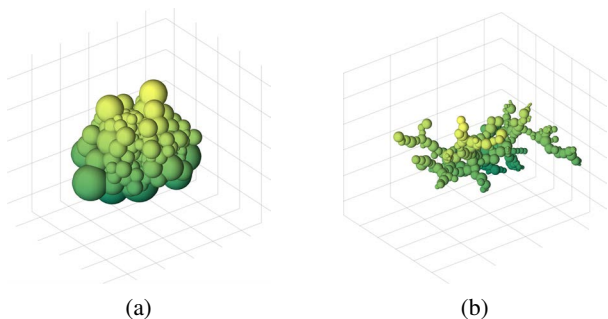


Fig. 13: Example of realizations of the GRAPE model with spherical particles which radius follows a log-normal distribution with a number of particles $N_p = 150$. Compact aggregate with $Z = 5$ (a) and unconstrained aggregate except for $Z \leq 2$ (b).

CONCLUSION

A stochastic geometrical model for compact aggregates has been proposed. Throughout this paper, it has been shown that it is possible, using an optimization process, to retrieve some of the 3D geometric characteristics of a compact aggregate from geometrical measurements made on a single 2D opaque projection image with, in most cases, less than 5% error. The GRAPE model is original in that it allows to adjust some 2D properties of the aggregates to be simulated. While the ability of the GRAPE model has been demonstrated in the context of estimating 3D properties of a compact aggregate, it has also been shown to be capable of generating many other types of aggregates, always with adjustable properties, such as string aggregates with specific lengths or tortuosities.

The areas of improvement are the application of these results to images of aggregates with unknown 3D properties, but also the extension of the method to non-convex aggregates, or even fiber-aggregates. It could also be interesting to try to aggregate sets of particles rather than assembling the particles one by one, with a cluster-cluster approach.

ACKNOWLEDGMENT

The author(s) acknowledge(s) the support of the French Agence Nationale de la Recherche (ANR), under grant ANR-20-CE07-0025 (project MORPHING).

REFERENCES

- Alander EM, Uusi-Penttilä MS, Åke C Rasmuson (2003). Characterization of paracetamol agglomerates by image analysis and strength measurement. *Powder Technol* 130:298–306.
- Atalar I, Yazici F (2019). Effect of different binders on reconstitution behaviors and physical, structural, and morphological properties of fluidized bed agglomerated yoghurt powder. *Drying Technol* 37:1656–64.
- Berg MJ, Sorensen CM (2013). Internal fields of soot fractal aggregates. *J Opt Soc Am A* 30:1947–55.
- Burd AB (2013). Modeling particle aggregation using size class and size spectrum approaches. *J Geophys Res Oceans* 118:3431–43.
- Bushell G, Yan Y, Woodfield D, Raper J, Amal R (2002). On techniques for the measurement of the mass fractal dimension of aggregates. *Adv Colloid Interface Sci* 95:1–50.

- de Langlard M, Lamadie F, Charton S, Debayle J (2021). Bayesian inference of a parametric random spheroid from its orthogonal projections. *Methodology and Computing in Applied Probability* 23:549–67.
- Deng X, Davé RN (2017). Breakage of fractal agglomerates. *Chem Eng Sci* 161:117–26.
- Dong Z, Liu Z, Wang P, Gong X (2017). Nanostructure characterization of asphalt-aggregate interface through molecular dynamics simulation and atomic force microscopy. *Fuel* 189:155–63.
- Einar Kruis F, van Denderen J, Buurman H, Scarlett B (1994). Characterization of agglomerated and aggregated aerosol particles using image analysis. *Part Part Syst Char* 11:426–35.
- Falconer K (1990). *Fractal geometry - mathematical foundations and applications*. Wiley.
- Faria N, Pons M, Feyo de Azevedo S, Rocha F, Vivier H (2003). Quantification of the morphology of sucrose crystals by image analysis. *Powder Technol* 133:54–67.
- Ferri G, Moreaud M, Humbert S, Digne M, Schweitzer JM (2021). Simulation of large aggregate particles system with a new morphological model. *IAS* 40:71–84.
- Florio BJ, Fawell PD, Small M (2019). The use of the perimeter-area method to calculate the fractal dimension of aggregates. *Powder Technol* 343:551–9.
- Frei M, Kruis FE (2018). Fully automated primary particle size analysis of agglomerates on transmission electron microscopy images via artificial neural networks. *Powder Technol* 332:120–30.
- Garboczi E (2002). Three-dimensional mathematical analysis of particle shape using x-ray tomography and spherical harmonics: Application to aggregates used in concrete. *Cem Concr Res* 32:1621–38.
- Gmachowski L (2002). Calculation of the fractal dimension of aggregates. *Colloids Surf, A* 211:197–203.
- Gong F, Liu Y, You Z, Zhou X (2021). Characterization and evaluation of morphological features for aggregate in asphalt mixture: A review. *Constr Build Mater* 273:121989.
- Guesnet E, Dendievel R, Jauffrès D, Martin C, Yrieix B (2019). A growth model for the generation of particle aggregates with tunable fractal dimension. *Physica A* 513:63–73.
- Guérin L, Coufort-Saudejaud C, Liné A, Frances C (2017). Dynamics of aggregate size and shape properties under sequenced flocculation in a turbulent taylor-couette reactor. *J Colloid Interface Sci* 491:167–78.
- Guérin L, Frances C, Liné A, Coufort-Saudejaud C (2019). Fractal dimensions and morphological characteristics of aggregates formed in different physico-chemical and mechanical flocculation environments. *Colloids Surf, A* 560:213–22.
- Henry C, Minier JP, Pozorski J, Lefèvre G (2013). A new stochastic approach for the simulation of agglomeration between colloidal particles. *Langmuir* 29:13694–707.
- Huo Y, Liu T, Liu H, Ma CY, Wang XZ (2016). In-situ crystal morphology identification using imaging analysis with application to the l-glutamic acid crystallization. *Chem Eng Sci* 148:126–39.
- Hussain M, Peglow M, Tsotsas E, Kumar J (2014). Modeling of aggregation kernel using monte carlo simulations of spray fluidized bed agglomeration. *AIChE J* 60:855–68.
- Jeldres RI, Concha F, Toledo PG (2015). Population balance modelling of particle flocculation with attention to aggregate restructuring and permeability. *Adv Colloid Interface Sci* 224:62–71.
- Jin C, Zou F, Yang X, You Z (2019). 3d quantification for aggregate morphology using surface discretization based on solid modeling. *J Mater Civ Eng* 31:04019123.
- Kadota K, Yamamoto T, Shimosaka A, Shirakawa Y, Hidaka J, Kouzu M (2011). Aggregation modeling of calcium carbonate particles by Monte Carlo simulation. *J Nanopart Res* 13:7209–18.
- Kaye BH (1994). *A random walk through fractal dimensions*. New York: VCH, 2nd ed.
- Kindratenko VV, Van Espen PJM, Treiger BA, Van Grieken RE (1996). Characterisation of the shape of microparticles via fractal and fourier analyses of scanning electron microscope images. In: Benoit D, Bresse JF, Van't dack L, Werner H, Wernisch J, eds., *Microbeam and Nanobeam Analysis*. Vienna: Springer Vienna.
- Komba JJ, Anochie-Boateng JK, van der Merwe Steyn W (2013). Analytical and laser scanning techniques to determine shape properties of aggregates. *Transp Res Rec* 2335:60–71.
- Lapuerta M, Barba J, Sediako AD, Kholghy MR, Thomson MJ (2017). Morphological analysis of soot agglomerates from biodiesel surrogates in a coflow burner. *J Aerosol Sci* 111:65–74.
- Lazzari S, Nicoud L, Jaquet B, Lattuada M, Morbidelli M (2016). Fractal-like structures in colloid science. *Adv Colloid Interface Sci* 235:1–13.

- Li J, Du Q, Sun C (2009). An improved box-counting method for image fractal dimension estimation. *Pattern Recognit* 42:2460–9.
- Li J, Huang L, Huang S (2021). Optimisation of aggregate gradation of ultra-high-performance concrete based on the modified compressible packing model. *Mag Concr Res* 73:1025–32.
- Li J, Zhang J, Qian G, Zheng J, Zhang Y (2019). Three-dimensional simulation of aggregate and asphalt mixture using parameterized shape and size gradation. *J Mater Civ Eng* 31:04019004.
- Liu H, Sun Z, Li W, Huyan J, Guo M, Hao X (2020). Evaluating angularity of coarse aggregates using the virtual cutting method based on 3d point cloud images. *IEEE Access* 8:143241–55.
- Maggi F, Bandera A, DeLuca LT, Thoorens V, Trubert JF, Jackson TL (2011). Agglomeration in solid rocket propellants: novel experimental and modeling methods. *Adv in AeroSpa Sci* 2:81–98.
- Maggi F, DeLuca LT, Bandera A (2015). Pocket model for aluminum agglomeration based on propellant microstructure. *AIAA J* 53:3395–403.
- McNaught AD, Wilkinson A (1997). *Compendium of Chemical Terminology. IUPAC Nomenclature Books Series ("Color Books")*. Oxford: Blackwell Science, 2nd ed.
- Mehle A, Likar B, Tomažević D (2017). In-line recognition of agglomerated pharmaceutical pellets with density-based clustering and convolutional neural network. In: 2017 Fifteenth IAPR International Conference on Machine Vision Applications (MVA).
- Monchot P, Coquelin L, Guerroudj K, Feltin N, Delvallée A, Crouzier L, Fischer N (2021). Deep learning based instance segmentation of titanium dioxide particles in the form of agglomerates in scanning electron microscopy. *Nanomaterials* 11.
- Morán J, Fuentes A, Liu F, Yon J (2019). Fracval: An improved tunable algorithm of cluster–cluster aggregation for generation of fractal structures formed by polydisperse primary particles. *Comput Phys Commun* 239:225–37.
- Morán J, Yon J, Poux A (2020). Monte carlo aggregation code (mca) part 1: Fundamentals. *J Colloid Interface Sci* 569:184–94.
- Omar W (2020). Experimental investigations of adipic acid agglomeration behavior under different operating conditions using image analysis technique qicpic software. *Part Sci Technol* 38:740–6.
- Ono K, Matsukawa Y, Saito Y, Matsushita Y, Aoki H, Era K, Aoki T, Yamaguchi T (2015). Monte Carlo simulation for morphology of nanoparticles and particle size distributions: comparison of the cluster–cluster aggregation model with the sectional method. *J Nanopart Res* 17:242.
- Pons M, Plagnieux V, Vivier H, Audet D (2005). Comparison of methods for the characterisation by image analysis of crystalline agglomerates: The case of gibbsite. *Powder Technol* 157:57–66.
- Ramkrishna D (2000). *Population balances: Theory and applications to particulate systems in engineering*. Acad Press.
- Ros F, Guillaume S, Sevilla F (1993). Agglomerates processing on in-flight images of granular products. In: Breidenthal SS, Desrochers AA, eds., *Vision, Sensors, and Control for Automated Manufacturing Systems*, vol. 2063. International Society for Optics and Photonics, SPIE.
- Rühle B, Krumrey JF, Hodoroba VD (2021). Workflow towards automated segmentation of agglomerated, non-spherical particles from electron microscopy images using artificial neural networks. *Sci Rep* 11:4942.
- Samson RJ, Mulholland GW, Gentry JW (1987). Structural analysis of soot agglomerates. *Langmuir* 3:272–81.
- Schmid HJ, Tejwani S, Artelt C, Peukert W (2004). Monte Carlo simulation of aggregate morphology for simultaneous coagulation and sintering. *J Nanopart Res* 6:613–26.
- Shen X, Lin M, Zhu Y, Ha HK, Fettweis M, Hou T, Toorman EA, Maa JPY, Zhang J (2021). A quasi-monte carlo based flocculation model for fine-grained cohesive sediments in aquatic environments. *Water Res* 194:116953.
- Shi Y, Wei J, Qiu J, Chu H, Bai W, Wang G (2020). Numerical study of acoustic agglomeration process of droplet aerosol using a three-dimensional cfd-dem coupled model. *Powder Technol* 362:37–53.
- Shyshko S, Mechtcherine V (2013). Developing a discrete element model for simulating fresh concrete: Experimental investigation and modelling of interactions between discrete aggregate particles with fine mortar between them. *Constr Build Mater* 47:601–15.
- Soille P (2003). *Morphological Image Analysis: Principles and Applications*. Berlin, Heidelberg: Springer-Verlag, 2nd ed.
- Song D, Jing D, Geng J, Ren Y (2015). A modified aggregation based model for the accurate prediction of particle distribution and viscosity in magnetic nanofluids. *Powder Technol* 283:561–9.

- Spetl A, Dosta M, Antonyuk S, Heinrich S, Schmidt V (2015). Statistical investigation of agglomerate breakage based on combined stochastic microstructure modeling and dem simulations. *Advanced Powder Technol* 26:1021–30.
- Suzuki M, Muguruma Y, Hirota M, Oshima T (1990). Fractal dimensions of particle projected shapes. *Advanced Powder Technol* 1:115–23.
- Thouy R, Jullien R (1994). A cluster-cluster aggregation model with tunable fractal dimension. *J Phys A: Math Gen* 27:2953–63.
- Tikhomirov VM (1993). ε -Entropy and ε -Capacity of Sets In Functional Spaces. Dordrecht: Springer Netherlands, 86–170.
- Tomchuk OV, Avdeev MV, Bulavin LA (2020). Modeling fractal aggregates of polydisperse particles with tunable dimension. *Colloids Surf, A* 605:125331.
- Turchiuli C, Castillo-Castaneda E (2009). Agglomerates structure characterization using 3d-image reconstruction. *Part Part Syst Char* 26:25–33.
- Wang Q, He J, Sun J, Ho J (2021). Determining the specific surface area of coarse aggregate based on sieving curve via image-analysis approach. *Constr Build Mater* 305:124728.
- Wentzel M, Gorzawski H, Naumann KH, Saathoff H, Weinbruch S (2003). Transmission electron microscopical and aerosol dynamical characterization of soot aerosols. *J Aerosol Sci* 34:1347–70.
- Zhang G, Zhang L, Wang J, Chi Z, Hu E (2018). A new multiple-time-step three-dimensional discrete element modeling of aerosol acoustic agglomeration. *Powder Technol* 323:393–402.
- Zheleznyakova AL (2021). A cost-effective computational approach based on molecular dynamics for generating 3d packs of irregularly-shaped grains in a container of complex geometry. *Powder Technol* 394:403–23.